Computational and Theoretical Chemistry 1117 (2017) 207–214

Contents lists available at ScienceDirect

Computational and Theoretical Chemistry

journal homepage: www.elsevier.com/locate/comptc

Real-time TD-DFT study on the dioxygen/superoxide radical charge transfer reaction

Aron Sc. Workman

Axoxy Laboratories, Gainesville, FL 32608, United States

ARTICLE INFO

Article history:
Received 13 June 2017
Received in revised form 18 August 2017
Accepted 19 August 2017
Available online 20 August 2017

Keywords:
Dioxygen/superoxide ($O_2/O_2^{\cdot-}$)
Charge transfer (CT)
Encounter complex (EC)
Time-dependent density functional theory (TD-DFT)

ABSTRACT

Superoxide (O_2^-) is an oxygen radical anion that damages biochemical systems. Here I executed real-time computations on the dioxygen/superoxide charge transfer (CT) reaction that is a mode of superoxide radical formation and propagation: ${}_aO_2 + {}_bO_2^- \rightarrow {}_aO_2^- + {}_bO_2$. Dioxygen/superoxide CT involves a diatomic oxygen dimer encounter complex (EC). I used time-dependent open shell density functional theory (TD-ODFT)/CAM−B3LYP to show that the parallel quartet EC had an optimized contact distance of 2.62 Å, and a fast oscillating free radical CT reaction time of 97.2 femtoseconds.

1. Introduction

Dioxygen (O_2) and superoxide ion ($O_2^{\cdot-}$) are reactive diatomic oxygen radicals. Dioxygen is a stable diradical and the most abundant oxygen allotrope on Earth that is essential to multitudinous chemical systems including those of atmospheric and oceanic chemistry (photosynthesis), electrochemistry (electrolysis), and biochemistry (aerobic respiration). Errors and missteps across these essential reactions and cascades can cause the formation of unstable superoxide radicals. The accumulation of superoxide radicals are minor concerns of atmospheric/marine chemistry and electrochemistry [1–4], and a major concern of biochemistry and medicine [5,6]. Linus Pauling commented on his discovery of superoxide radical with: "it is a source of satisfaction to me that the superoxide radical, whose existence was predicted through arguments based upon the theory of quantum mechanics, should have turned out to be important in biology and medicine" [7]. Computational quantum chemistry is utilized here to test hypotheses on superoxide radical formation, propagation, and dissipation.

The quantized configuration of dioxygen is $O_2(^3\Sigma_g^-)$: $\sigma_{1s}^2\sigma_{1s}^{*2}\sigma_{2s}^2\sigma_{2s}^{*2}\sigma_{2pz}^2\pi_{2py}^2\pi_{2px}^2\pi_{2py}^{*1}\pi_{2px}^{*1}\sigma_{2pz}^{*0}$, and the quantized configuration of superoxide is $O_2^-(^2\Pi_g)$: $\sigma_{1s}^2\sigma_{1s}^{*2}\sigma_{2s}^2\sigma_{2s}^{*2}\sigma_{2pz}^2\pi_{2py}^2\pi_{2px}^2\pi_{2py}^{*2}\pi_{2px}^{*1}\sigma_{2pz}^{*0}$. Both of these diatomic oxygen molecules have degenerate antibonding orbitals: π_{2py}^* and π_{2px}^*, which are responsible for their reactivity. Superoxide formation can occur with the vertical attachment of electron number 33 in the diatomic oxygen dimer. The charge transfer (CT) is a one-electron reduction with equation: $O_2 \xrightarrow{e^-} O_2^-$ [8,9]. The dioxygen/superoxide charge transfer reaction has equation: ${}_aO_2 + {}_bO_2^- \rightarrow {}_aO_2^- + {}_bO_2$. That reaction is one mode by which superoxide formation and dissipation regularly occurs.

Superoxide formation from and dissipation to dioxygen do not involve classical chemical bonding, therefore the transition states are key. Though the CT reaction has been described by five sequential steps [10,11], it can be effectively described with just two (excluding equilibrium and relaxation), which are characterized by 1. the appearance of the key formation of an encounter complex (EC) structure: ${}_aO_2 \cdots {}_bO_2^-$; and 2. the formation of an activated state: ${}_aO_2(r) \cdots {}_bO_2^-(r)$. The dioxygen/superoxide EC configuration can have a multiplicity of either two or four; doublet ECs differ in their properties from quartet ECs [10]. These reaction mechanisms are dependent on an EC structure. The EC may be of paramount importance to the rate and favorability of the dioxygen/superoxide CT reaction.

The dioxygen/superoxide CT reaction has been previously studied by other research groups [12-19]. Bu and coworkers found activation energies and coupling matrix elements for both the doublet and quartet states, and it was shown that the reaction is most likely to proceed by the quartet rather than doublet EC [10,11]. Indications show that the gas phase computations of this manuscript also have applicability to the liquid phase because dioxygen and superoxide do not leave the gaseous state except under extreme experimental circumstances [20,21].

E-mail address: aron@axoxy.com

http://dx.doi.org/10.1016/j.comptc.2017.08.020
2210-271X/

Superoxide radicals are a transient and reactive species not easily studied even with advanced experimental methodologies that require sophisticated reagents and instrumentation, such as particle accelerator pulse radiolysis, electron paramagnetic resonance spectroscopy, and cyclic voltammetry. Computational methodologies are currently the best method to obtain dioxygen and superoxide potential energy curves, and the sole method by which to investigate the femtosecond-scale reaction coordinates of the transition states, excepting specialist spectroscopy. In this study, the computational methodologies used were real-time TD-ODFT and ODFT as the modules, CCSD(T) and CAM-B3LYP as the *XC* functionals, and aug-cc-pVTZ and 6-311++G** as the basis sets. TD-ODFT is TD-DFT, except that the DFT is computed with the open-shell systems of ODFT (using spin-unrestricted wavefunctions).

2. Methods

2.1. Group theory

Diatomic oxygen is linear and centrosymmetric with a $D_{\infty h}$ point group designation, and a full rotation of $\Pi_g \otimes \Pi_g$ for $O_2(^3\Sigma_g^-)$ and $\Sigma_g^+ \otimes \Pi_g$ for $O_2^-(^2\Pi_g)$. Diatomic oxygen molecular orbitals (σ and π) have the reducible representation $\Gamma = \Sigma \oplus \Pi(\chi = 6)$. An abelian point group was necessary for symmetric computations, so a D_{2h} perturbation was assigned due to shared $D_{\infty h}$ operations $(E, 2C_2, C_2', 2\sigma_v, \sigma_h, i)$ [22]. $D_{\infty h}$ partial point group correlations were verified by computing the D_{2h} linear combination and their correlary wavefunctions. Breaking inversion symmetry by demoting D_{2h} to C_{2v} was explored [23], but did not have a discernible effect.

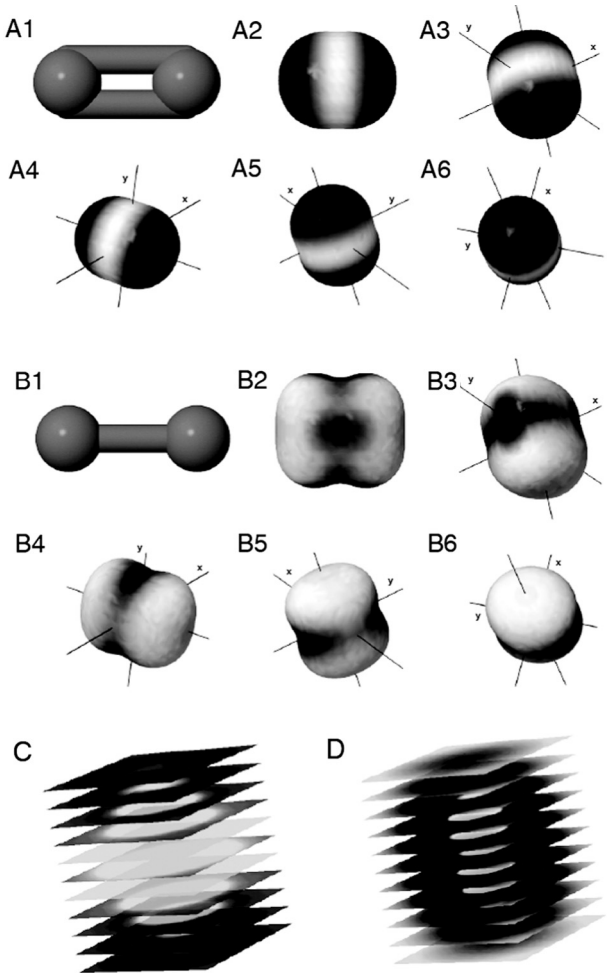

Fig. 1. Total isosurface renderings of (A, C) dioxygen and (B, D) superoxide. ODFT results computed at CAM-B3LYP/aug-cc-pCVQZ. (1) is a cartoon at the yz plane, (2) is also at the yz plane; (3–6) include axes. Each successive rendering (2–6) varies the wave cutoff from 0.0002 to 0.001 in 0.002 increments. (C, D) XY translucent planar slices of total isosurfaces with a wave cutoff of 0.0004.

2.2. ODFT and basis sets

Systems were computed in the gas phase implementing hybrid open-shell density functional theory (ODFT). A coulomb-attenuated (range-adjusted) functional was used to assess the CT system: CAM-B3LYP. CAM-B3LYP is a generalized gradient approximation hybrid *XC* exchange functional (Becke 1993), with Lee-Yang-Par's correlation, and a long-range Coulomb-attenuated correction that is explicitly defined for CT systems [24–27]. CAM-B3LYP computations implemented ODFT with spherical-harmonic angular basis sets. Several levels of theory (and with differing diffusions and polarizations) were impartially assayed using the python programming language. Double * and + were chosen rather than single * and + for continuing compatibility with other systems. Full optimization data sets were collected from the Dunning sets aug-cc-pVTZ and aug-cc-pCVQZ, and the Pople sets 6-31G**, 6-31++G**, and 6-311++G**. The primary basis sets implemented here were 6-311++G** and aug-cc-pVTZ [28,29]. A representative NWChem input file for the distance-energy calculations is:

```
python
  geometry = ""
    geometry noprint; symmetry d2 h
      O 0 0%f;
    end
  ""
  x = 0.1
  while (x < 2.0):
    input_parse(geometry% x)
    energy = task_energy('dft')
    print ' x =%f energy =%f'% (x, energy)
    x = x + 0.01
end
dft
  xc xcamb88 1.00 lyp 0.81 vwn_5 0.19 hfexch 1.00
  cam 0.33 cam_alpha 0.19 cam_beta 0.46
  odft
  convergence density 1 d-9
  grid fine
  maxiter 1000
  mult 3
end
  print none
  task python
```

2.3. Real-time TD-ODFT

The real-time charge kinetics of the dioxygen/superoxide CT reaction were obtained through real-time TD-ODFT [30]. The Kohn-Sham molecular orbitals of the ECs were integrated over time to generate oscillating charge graphs. First, the ground state density matrix was computed. Next, the density matrix was propagated utilizing the real-time TD-ODFT module. Lastly, the time-dependent observable (charge) was recorded as a function of time,

and graphed. A representative NWChem input file for the real-time TD-ODFT is:

```
start tcne
echo
geometry "bottom" units angstroms noautosym nocenter
  noautoz
o          0.67313          0          0
o          -0.67313         0          0
end
geometry "top" units angstroms noautosym nocenter noautoz
o          0.60309          2.62       0
o          -0.60309         2.62       0
end
dft
  xc xcamb88 1.00 lyp 0.81 vwn_5 0.19 hfexch 1.00
  cam 0.33 cam_alpha 0.19 cam_beta 0.46
  odft
  convergence density 1 d-7
  grid fine
  maxiter 1000
end
charge -1
set geometry "bottom"
dft
  mult 2
  vectors input atomic output "bottom.movecs"
end
task dft energy
charge 0
set geometry "top"
dft
  mult 3
  vectors input atomic output "top.movecs"
end
task dft energy
charge -1
set geometry "dimer"
dft
  mult 4
  vectors input fragment "bottom.movecs" "top.movecs"
  output "dimer.movecs"
  noscf
end
task dft energy
rt_tddft
  tmax 500.0
  dt 0.2
  load vectors "dimer.movecs"
  print dipole field energy s2 charge
end
task dft rt_tddft
```

2.4. Hardware and software

NWChem 6 software suite (with a tensor contraction engine and parallel OpenMPI support) with Python 2 was compiled from source with C/Fortran and executed on Linux operating systems [31,32]. An 8X/16GB box processed minor preliminary calculations and most geometric optimizations, and to queue the main computations including the real-time TD-ODFT.

3. Results and discussion

3.1. Diatomic oxygen radicals – dioxygen and superoxide

3.1.1. Renderings of the total isosurfaces

Dioxygen and superoxide were first studied independent of the EC and their CT reaction. Dioxygen and superoxide were computed in a three-dimensional Hilbert space with the *x*-axis as the equatorial parallel. A visual depiction of the optimized molecular structures of these two diatomic oxygen radicals were given by the isosurfaces of Fig. 1.

3.1.2. Potential energy curves with energetic minimums

Potential energy curves and definitive energetic minimums for dioxygen and superoxide have been experimentally determined by rotational spectroscopy with a consensus for the lowest total

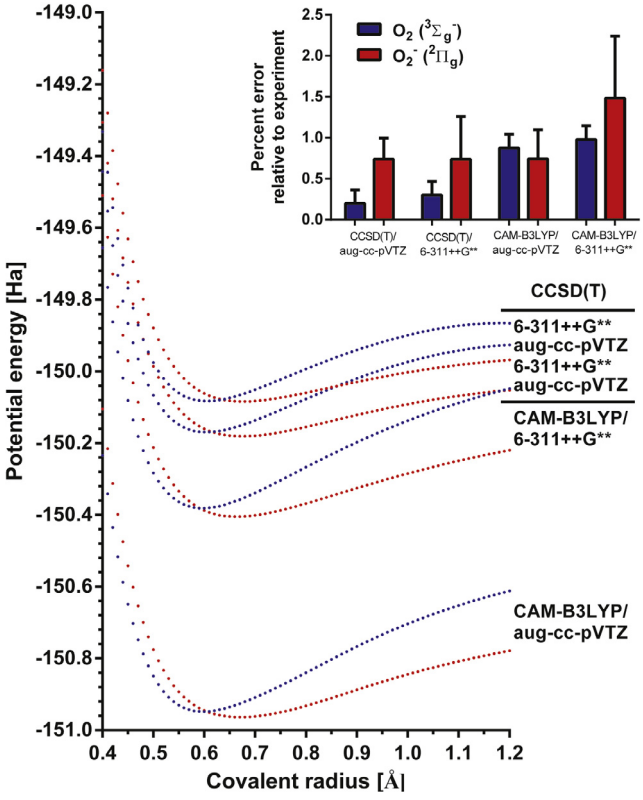

Fig. 2. Potential energy curves of dioxygen (blue) and superoxide (red). Computed at the CCSD(T) and CAM-B3LYP levels of theory. Inset: percent errors relative to CRC/NIST. (For interpretation of the references to colour in this figure legend, the reader is referred to the web version of this article.)

Table 1
Energetic minimums from the geometric optimizations of dioxygen and superoxide at several different levels of theory. The CAM-B3LYP, CCSD(T), EOM-CCSDT, and MP2 levels of theory utilized the variable basis sets. Included in part for internal consistency, this data was drawn from a different version of NWChem (6.5) than the rest of the manuscript (6.3).

Level of theory	Dioxygen [Ha]	Superoxide [Ha]
CAM-B3LYP/6-311++G	−150.38	−150.41
CAM-B3LYP/ aug-cc-pVTZ	−150.38	−150.38
CCSD(T)/6-311++G	−150.08	−150.07
EOM-CCSDT/6-311++G**	−149.83	−149.88
MP2	−150.38	−150.24

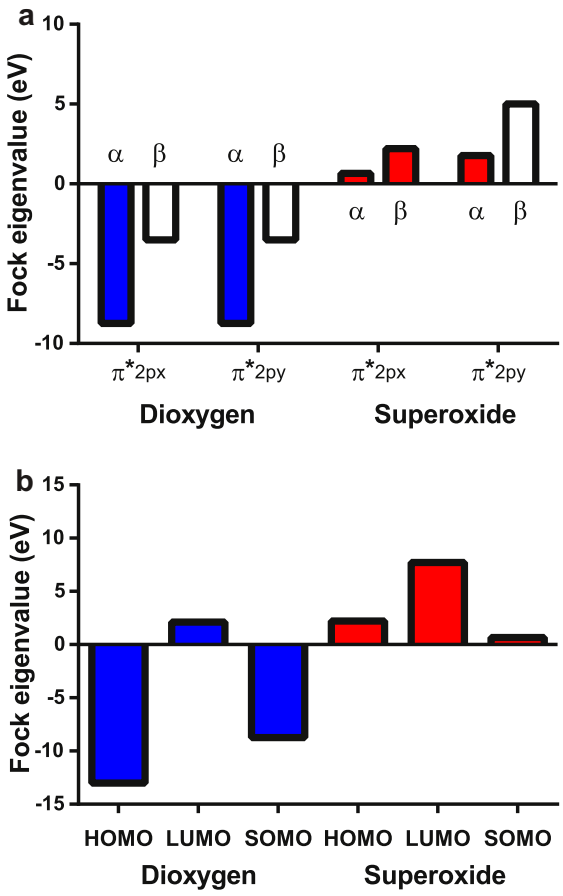

Fig. 3. ODFT potential energies of the valent molecular orbitals of dioxygen and superoxide. (a) Specific energies of the degenerate anti-bonding oxygen orbitals responsible for the reactivity computed at CAM-B3LYP/6-311++G**, and (b) optimized vertical detachment input ionization potentials of dioxygen and superoxide (d = 3 Å) computed at CAM-B3LYP/aug-cc-pVTZ. A filled bar indicates an orbital filled with an electron and an empty bar indicates an orbital not filled with an electron.

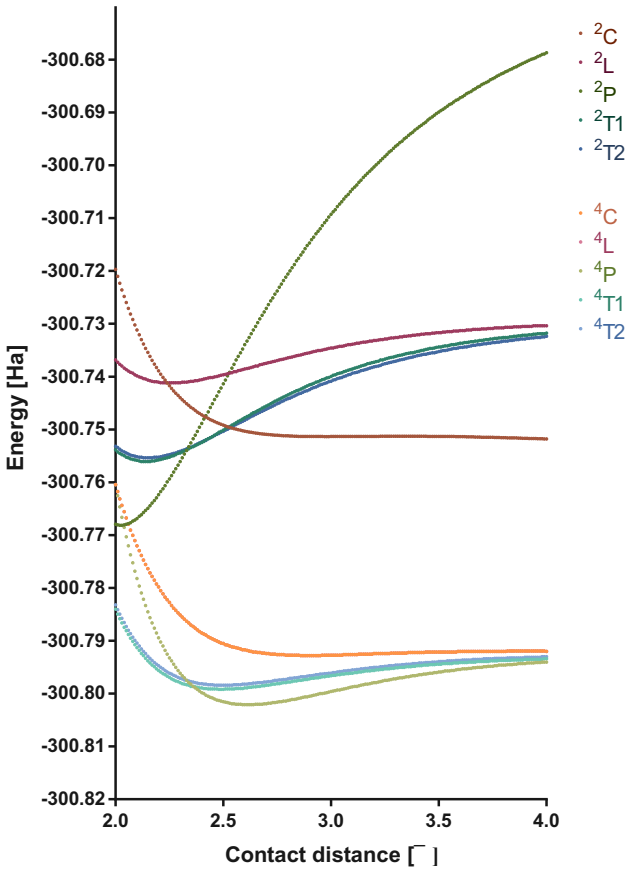

Fig. 4. Potential energies of the doublet (2) and quartet (4) ECs as a function of intermolecular contact distance. ODFT results were computed at CAM-B3LYP/aug-cc-pVTZ. (P) parallel, (L) collinear, (C) crossing, (T1) t-type I, and (T2) t-type II.

energy and optimum intramolecular distance [33–37]. Relevant computational studies continue to work toward higher resolutions and lower percent errors. Here I provide potential energy minimums and curves for both species at 0.01 Å resolution, and at several different levels of theory. Fig. 2 shows the potential energy curves of dioxygen and superoxide, which have high resolution and low percent error using the experimental results of rotational spectroscopy (CRC/NIST data). The energetic minimum of dioxygen was −150.37209 Ha at 0.60309 Å, and the energetic minimum of superoxide was −150.39349 Ha at 0.67313 Å when computed with the most accurate *XC* functional, which was CCSD(T), in this case. The total potential energy of superoxide intersects that of dioxygen at its geometric minimum, which has implications for the activated state.

Each level of theory shown had an approximation error of <1% for dioxygen and <2.5% for superoxide relative to CRC/NIST (rotational spectroscopy experiments): $O_2(^3\Sigma_g^-)$ = 0.602–0.604 Å [33], and $O_2^-(^2\Pi_g)$ = 0.668–0.678 Å [38]. Spin-paired orbitals had high overlap at >96% (and typically 98–100%), and energetic variation from exact repetition or computation alone (spin designation, etc.) was negligible (<0.002%). Dunning geometric optimizations that preceded Pople energetics computations did not limit that error. Switching the initial value of the radius from 0.01 to 10 Å did not limit that error. Increasing the number of SCF optimization iterations from 50 to 10,000 did not limit that error. A few computations tested the unrestricted MP2 functional following the findings of a previous publication [15], but CAM-B3LYP stood more accurate within NWChem. 6-31++G** alleviates that basic error seen in a prior publication which used 6-31G** instead. CCSD(T) validated certain computations [39]. EOM-CCSDT was more expensive than, yet produced nearly equivalent data points to, CCSD(T).

Table 2
The encounter complex structure coordinates by atom. Consider an equatorial parallel x-axis. The intramolecular contact distances are r_a and r_b, and the intermolecular contact distance is d.

Molecule	Dioxygen						Superoxide					
Atom	O			O			O			O		
Coord.	x	y	z	x	y	z	x	y	z	x	y	z
Parallel	r_a	$-d/2$	0	$-r_a$	$-d/2$	0	r_b	$d/2$	0	$-r_b$	$d/2$	0
Linear	$-d/2$	0	0	$-2r_a - d/2$	0	0	$d/2$	0	0	$2r_b + d/2$	0	0
Crossing	0	r_a	$-d/2$	0	$-r_a$	$-d/2$	r_b	0	$d/2$	$-r_b$	0	$d/2$
T-type 1	$-d/2$	r_a	0	$-d/2$	$-r_a$	0	$d/2$	0	0	$2r_b + d/2$	0	0
T-type 2	$d/2$	0	0	$2r_a + d/2$	0	0	$-d/2$	r_b	0	$-d/2$	$-r_b$	0

EOM-CCSDT/aug-cc-pVTZ had the lowest percent error yet reported for dioxygen at 0.017%, but superoxide did not easily converge under the same symmetry. Minimum energies for dioxygen and superoxide using CCSD(T) and CAM-B3LYP compared to EOM-CCSDT and MP2 are given in Table 1.

3.1.3. Electron potentials of the HOMOs, LUMOs, and SOMOs

The proposed mechanism is the EC and its activated state rather than simplistic detachment from superoxide and attachment to dioxygen. Still, as a potential alternative, specific attention was owed to the molecular orbital electron attachment and detachment energies, which were given in Fig. 3. Dioxygen attachment

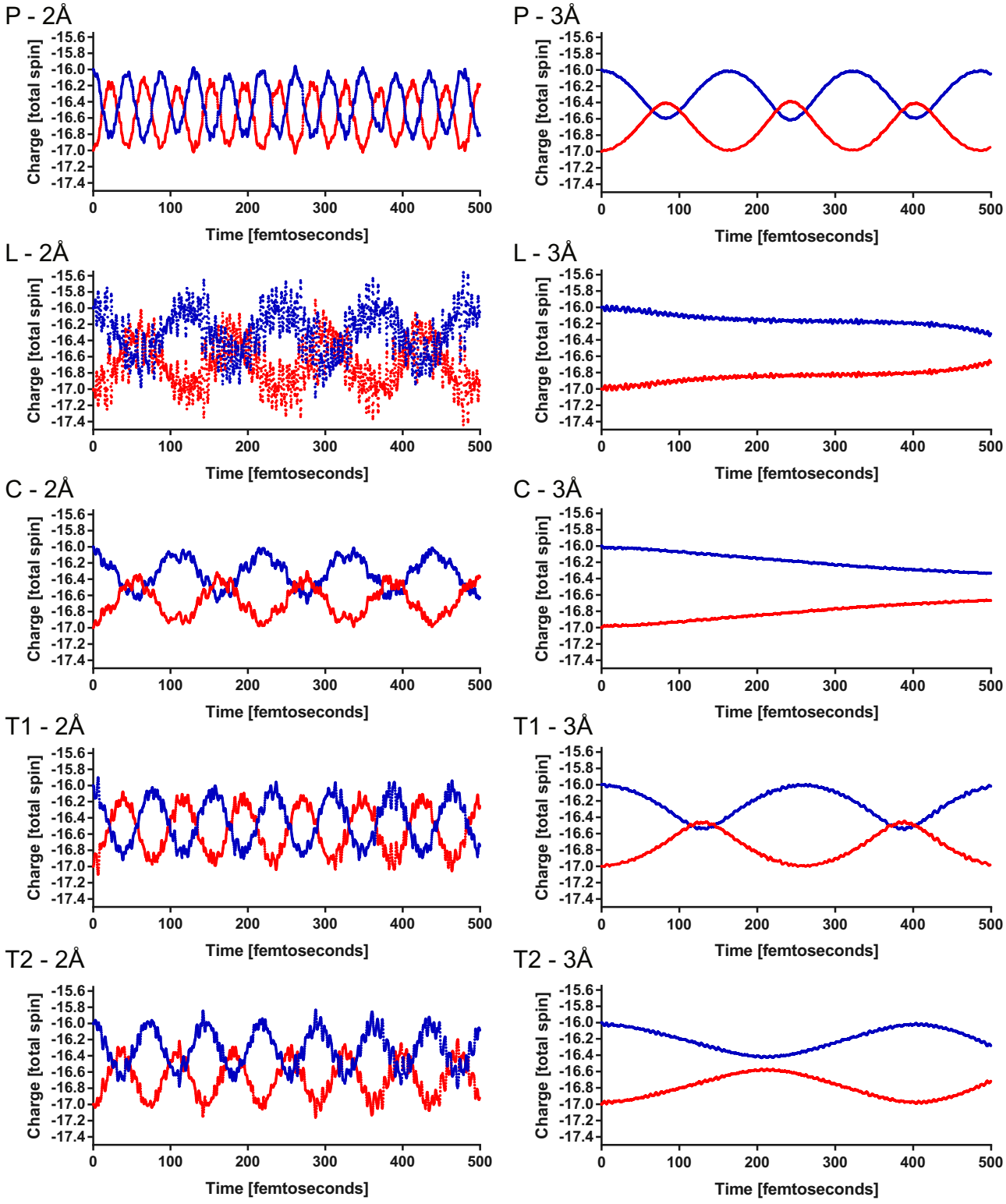

Fig. 5. Real-time TD-ODFT results of the CT reaction of the five quartet ECs at intermolecular contact distances of 2 Å and 3 Å. To-scale graphs at 0.2 fs intervals. Real-time TD-ODFT results were computed at CAM-B3LYP/aug-cc-pVTZ. (P) parallel, (L) collinear, (C) crossing, (T1) t-type I, and (T2) t-type II. Blue is the molecule that begins the reaction as dioxygen and red is the molecule that begins the reaction as superoxide.

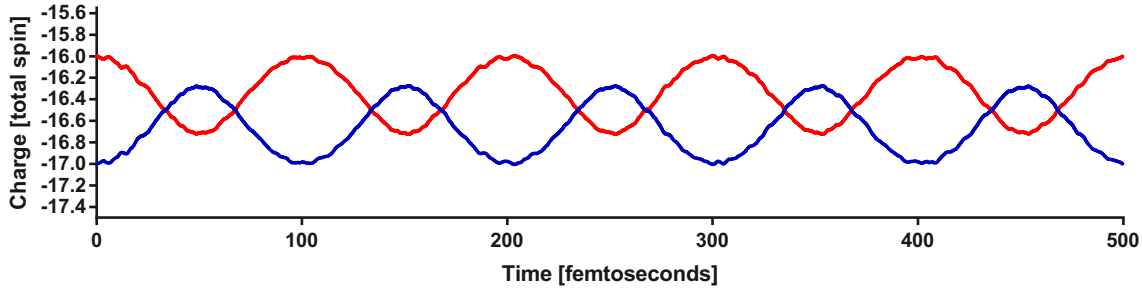

Fig. 6. Real-time TD-ODFT results of the CT reactions for the quartet parallel EC structure at optimized contact distance. Contact distances to maximum times of (a) 2.62 Å to 500 fs. Real-time TD-ODFT results were computed at CAM-B3LYP/aug-cc-pVTZ. Blue is the molecule that begins the reaction as dioxygen and red is the molecule that begins the reaction as superoxide. (For interpretation of the references to colour in this figure legend, the reader is referred to the web version of this article.)

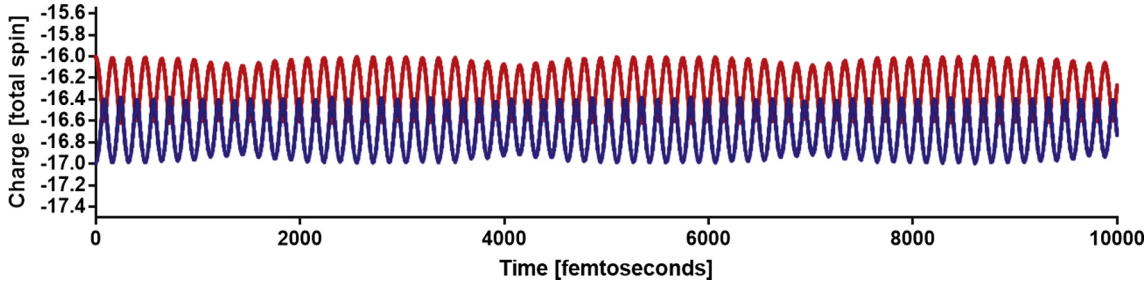

Fig. 7. Real-time TD-ODFT results of the CT reactions for the quartet parallel EC structure. Contact distances to maximum times of 3 Å to 10 ps. Real-time TD-ODFT results were computed at CAM-B3LYP/aug-cc-pVTZ. Blue is the molecule that begins the reaction as dioxygen and red is the molecule that begins the reaction as superoxide. (For interpretation of the references to colour in this figure legend, the reader is referred to the web version of this article.)

forms superoxide. Superoxide detachment forms singlet dioxygen, and superoxide attachment forms peroxide. Ionizing detachment from the superoxide highest occupied molecular orbital (HOMO) is favorable whereas ionizing detachment from the dioxygen HOMO is not. For the HOMO vertical detachment, dioxygen error was approximately 7% relative to the CRC experimental value [40], which was below par for DFT vertical detachment approximation errors. Ionizing attachment to the lowest unoccupied molecular orbital (LUMO), which was σ^*_{2pz} for diatomic oxygens, is also not favorable. Both detachment from and attachment to the SOMO, which is π^*_{2p} for diatomic oxygen, are energetically favorable. Superoxide SOMO detachment forms $O_2(^1\Delta_g)$ (singlet dioxygen) with favorability −0.1536 eV, and superoxide SOMO attachment forms $O_2^{2-}(^1\Sigma_g^+)$ (peroxide) with favorability −6.717 eV. Both detachment from and attachment to superoxide are favorable, however attachment is considerably more favorable than detachment, indicating attachment reduction to peroxide is more predominant than detachment oxidation back to dioxygen. These computational measurements are of the stable chemical species and not the transient radical species that is most likely to occur in a physical context. It is probably safe to conclude that the dioxygen/superoxide CT reaction is not the result of a two-step detachment from superoxide followed by attachment to dioxygen; an EC transition state is apparently necessary for this specific CT reaction.

3.2. Doublet and quartet dioxygen/superoxide encounter complexes

3.2.1. The encounter complexes

The doublet and quartet ECs including the resultant activated state will now be addressed. The dioxygen/superoxide CT reaction proceeds by 1. an EC: ${}_aO_2 \cdots {}_bO_2^-$; and 2. an activated state: ${}_aO_2(r) \cdots {}_bO_2^-(r)$. The EC geometry partially determines the favorability of the CT reaction. The EC can hold a number of structures. Five structures with an intramolecular covalent radius (r) and intermolecular contact distance (d) were geometrically oriented as either parallel (P), collinear (L), crossing (C), or T-type (T1 and T2) [10], as defined in Table 2. Furthermore, the EC configuration can have a multiplicity of either two or four (doublet or quartet).

3.2.2. Potential energy curves with energetic minimums

Two unique approaches were used to compute the potential energy curves of the ECs. 1. The electrons were placed at the appropriate occupancies for either the doublet or quartet multiplicity using the NWChem 'swap vector' option, and electron number 33 in the diatomic oxygen system was correctly identified, as confirmed by density analyses [41,42]. 2. To test continuity of theory by a different approach, an *ab initio* LCAO-MO method was equipped: the two by two oxygen atoms were geometrically assembled, the applied charge of electron number 33 was assigned to the system, and the four atoms were then combined as a dimer. The results from the *ab initio* method (approach 2) did not substantially differ from the results of the software-established module (approach 1). The total potential energies of the doublet and quartet ECs are now given in Fig. 4.

The quartet ECs had lower energy and more definitive metrics than the doublet ECs: quartet EC energies converge whereas doublet EC energies diverge as the contact distance increases. The homogeneous quartet ECs had lower energy and the shape of their potential energy curves were more consistent than that of the heterogeneous doublet ECs. Here I have used an entirely different system to confirm finding that the dioxygen/superoxide CT reaction is most likely to occur via the quartet rather than the doublet state [10]. The energetic minimums of the dioxygen/superoxide ECs were found utilizing a python iteration. For the quartet state, the optimum contact distances for the five ECs were 2.91 Å for crossing (^{4}C), 2.55 Å for collinear (^{4}L), 2.62 Å for parallel (^{4}P), 2.49 Å for T-type I (^{4}T1), and 2.50 Å for T-type II (^{4}T2). The exactitude of the radial computations superseded the previously reported highest resolution of "∼3 Å" in all cases. All quartet structures reached an energetic minimum below −300.9 Ha. The quar-

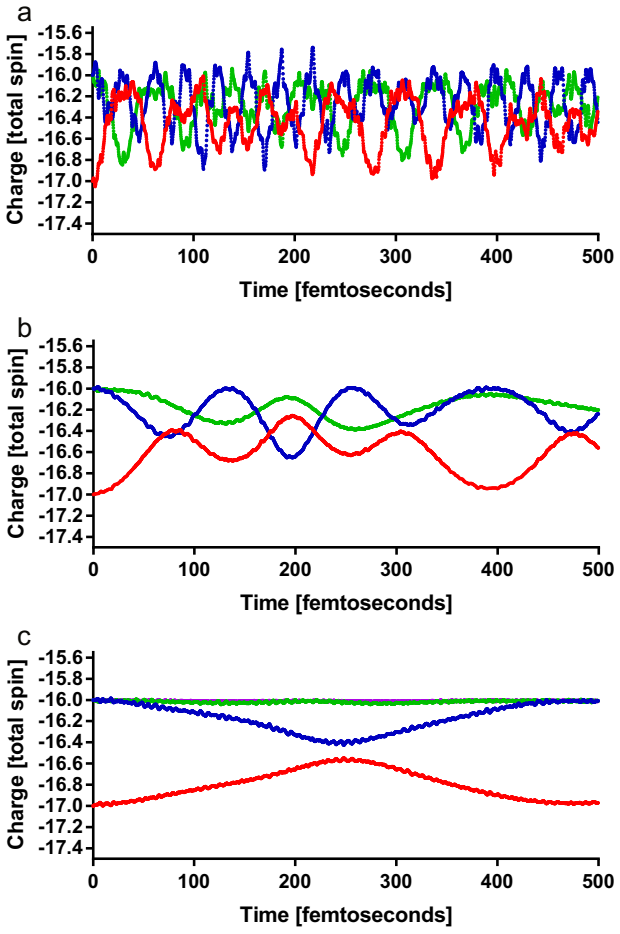

Fig. 8. Real-time TD-ODFT results of the CT reactions with a third oxygen atom in the quartet parallel EC structure. Contact distances and number of oxygen atoms of (a) 2 Å and 3 oxygen atoms total, (b) 3 Å and 3 oxygen atoms total, (c) 3 Å and 4 oxygen atoms total. Real-time TD-ODFT results were computed at CAM-B3LYP/aug-cc-pVTZ. Blue and green are the molecular structures that begin the reaction as dioxygen and red is the molecular structure that begins the reaction as superoxide. (For interpretation of the references to colour in this figure legend, the reader is referred to the web version of this article.)

tet parallel EC structure – which was the most energetically favorable EC structure studied – reached an absolute minimum at −300.8021 Ha.

3.2.3. The activated transition state structure

The results hitherto give enough information to build a theory about the activated state and its potential role as another transition state in the dioxygen/superoxide CT reaction. The activated state precedes the completion of one cycle of the CT reaction. The activated state is the transition structure that follows from the EC structure. During the course of the CT reaction, the EC structure may proceed to pair with adjacent diatomic oxygen species in series in order to transfer the charge to another molecule, according to the net equation: ${}_aO_2 + {}_bO_2^- \rightarrow {}_aO_2^- + {}_bO_2$. An energetic equilibrium may control the CT reaction according to the equation: $E_{activation} = E({}_aO_2(r)) + E({}_bO_2^-(r))$.

3.3. Real-time quartet dioxygen/superoxide charge transfer reactions

3.3.1. The five encounter complexes at two contact distances

After the EC structures were adequately delineated, I computed the superoxide CT reaction in real-time using TD-ODFT. A dioxygen/superoxide EC structure was programmatically loaded. The oscillations of electron number 33 were then observed (without an applied electric field). The results became predictable and consistent: electron number 33 is transferred homogeneously that varies with EC geometry. Results at the contact distances of 2 Å and 3 Å were graphed as shown in Fig. 5. These CT studies in real-time show that electron number 33 begins on one diatomic oxygen molecule and then fully transfers to the other diatomic oxygen molecule, generating a state that is easily described as superoxide. The frequency of the observed charge oscillation is dependent on the geometric arrangement of the EC structure including the intermolecular contact distance between the two diatomic oxygen molecules. The CT over real-time has both a more consistent amplitude and a greater frequency with decreasing contact distance for each EC structure, indicating that the CT reaction is completed both fuller and faster as the diatomic oxygen molecules gain proximity in space. The collinear EC structure is not precise relative to the other ECs. This lack of precision is reproducible and apparently an attribute of the geometric arrangement.

3.3.2. Parallel encounter complex at its optimized contact distance

I next sought to test the quartet ECs at their optimized contact distances, which have minimum energy. Accumulated data at different contact distances gave me an interest in the quartet parallel EC structure, which has an optimized contact distance of 2.62 Å. The real-time CT results are given in Fig. 6. At the quartet parallel EC structure with the optimized contact distance, the superoxide CT reaction occurs at a rate of 97.2 fs, which is the rate at which the charge oscillates across the diatomic oxygen molecules in series.

3.3.3. Parallel encounter complex up to ten picoseconds

The electric charge oscillates for the duration of the reaction, even when observed for up to 10 picoseconds, as given in Fig. 7. After observing the CT reaction up to 10 ps, a secondary oscillation pattern emerged at a rate of approximately 2.25 ps. Given just two diatomic oxygen molecules in series, the CT reaction always had precise sinusoidal symmetry. Using this system, I was able to determine the frequency with which the charge was transferred.

3.3.4. Spontaneous dismutation with a third and fourth oxygen atom

To expand on these experiments, I began computing more than two diatomic oxygen molecules in series by rigid geometric constructions, as shown in Fig. 8. Spontaneous dismutation to peroxide probably occurred when multiple species (three or four diatomic oxygen molecules total rather than just two) were computed in series, or the geometric configurations were not accurate enough to proceed into dismutation chemistry.

4. Conclusion

An understanding of the most prevalent electron acceptor that is dioxygen, and the reaction which spurns it to radicalize, is of paramount importance to several fundamental and applied sciences, most notably aerobic biochemistry.

In this work, ODFT and real-time TD-ODFT computed with CCSD (T) and CAM-B3LYP as the *XC* functional were used to compute the dioxygen/superoxide CT reaction as a model of superoxide radical formation and propagation. The CCSD(T) computations yielded dioxygen and superoxide geometric optimizations with very high accuracy and low percent error (relative to rotational spectroscopy experiments). This manuscript determined the optimum contact distances for the structures of the EC of the dioxygen/superoxide CT reaction. This manuscript is first to apply TD-DFT to the dioxygen/superoxide CT reaction. I found that the favorability of the CT reaction is a function of the EC. Of the five (ten including multiplic-

ity) possible structures studied here, the CT reaction almost certainly proceeds via the quartet parallel EC structure, but this was already known.

The electron flux may proceed by the picosecond in an adiabatic cyclic or chain reaction. The extra electron that characterizes superoxide as a distinct state from dioxygen has high ionic mobility. The resultant instantaneous point-charged specie is called superoxide. The real-time TD-ODFT computations here show that superoxide is well-described as dioxygen with a near-instantaneous point charge. Superoxide is substantially abundant as a state of dioxygen. Superoxide radicals were once viewed as a sparse species, but they are considerably more abundant than the literature suggests.

The radical is an upstream 'reactive oxygen species' that indicate a chemical imbalance called oxidative stress. Oxidative stress is associated with deleterious physiology including inflammatory signaling cascades, cell proliferation and angiogenesis or cancers, lipid peroxidation and protein oxidation, nuclear and mitochondrial DNA mutation, and apoptosis/necrosis or cellular death, leading some researchers to theorize about the 'free radical theory of aging'. Therefore, studies on the quantum chemistry of superoxide radical are of interest to many applied sciences, including those sustaining the free radical theory of aging and disease.

References

[1] Y. Shaked, A. Rose, Seas of superoxide, Science 340 (2013) 1176.
[2] H. Yang, R.L. McCreery, Elucidation of the mechanism of dioxygen reduction on metal-free carbon electrodes, J. Electrochem. Soc. 147 (2000) 3420.
[3] J.P. Roth, R. Wincek, G. Nodet, D.E. Edmondson, W.S. McIntire, J.P. Klinman, Oxygen isotope effects on electron transfer to O2 probed using chemically modified flavins bound to glucose oxidase, J. Am. Chem. Soc. 126 (2004) 15120.
[4] V.S. Bryantsev, V. Giordani, W. Walker, M. Blanco, S. Zecevic, K. Sasaki, J. Uddin, D. Addison, G.V. Chase, Predicting solvent stability in aprotic electrolyte Li–air batteries: nucleophilic substitution by the superoxide anion radical (O2•–), J. Phys. Chem. A. 115 (2011) 12399.
[5] I. Fridovich, Superoxide radical: an endogenous toxicant, Annu. Rev. Pharmacol. Toxicol. 23 (1983) 239.
[6] A.W. Rutherford, A. Osyczka, F. Rappaport, Back-reactions, short-circuits, leaks and other energy wasteful reactions in biological electron transfer: redox tuning to survive life in O 2, FEBS Lett. 586 (2012) 603.
[7] L. Pauling, The discovery of the superoxide radical, Trends Biochem. Sci. 4 (1979) N270.
[8] A. Ignaczak, W. Schmickler, S. Bartenschlager, Electrochemical reduction of the O 2 molecule to the radical ion–a theoretical approach, J. Electroanal. Chem. 586 (2006) 297.
[9] J. Lind, X. Shen, G. Merenyi, B. Jonsson, Determination of the rate constant of self-exchange of the oxygen O2/O2-couple in water by 18O/16O isotope marking, J. Am. Chem. Soc. 111 (1989) 7654.
[10] Y. Bu, Y. Wang, H. Sun, C. Deng, Structure and property study of the O 2 O 2− electron transfer system, J. Molec. Struct.: THEOCHEM. 429 (1998) 143.
[11] Y. Bu, D. Zhou, Q. Zhou, C. Deng, Golden-rule treatment of the O2 + O2- electron-transfer reaction, J. Mol. Struct. THEOCHEM. 459 (1999) 177.
[12] Y.A. Ilan, G. Czapski, D. Meisel, The one-electron transfer redox potentials of free radicals, I. The oxygen/superoxide system, Biochim. Biophys. Acta Bioenergetics 430 (1976) 209.
[13] M.S. McDowell, J.H. Espenson, A. Bakac, Kinetics of aqueous outer-sphere electron-transfer reactions of superoxide ion: implications concerning the dioxygen/superoxide (O2/O2-)self-exchange rate constant, Inorg. Chem. 23 (1984) 2232.
[14] E.D. German, A.M. Kuznetsov, I. Efremenko, M. Sheintuch, Theory of the self-exchange electron transfer in the dioxygen/superoxide system in water, J. Phys. Chem. A 103 (1999) 10699.
[15] Y. Wang, X. Zhang, Y. Liu, Q. Zhang, Ab initio studies on the electron transfer O∼ 2 O∼ 2^.^-→ O∼ 2^.^- O∼ 2, Acta Chim. Sinica 58 (2000) 19.
[16] K.M. Rosso, J.J. Morgan, Outer-sphere electron transfer kinetics of metal ion oxidation by molecular oxygen, Geochim. Cosmochim. Acta 66 (2002) 4223.
[17] J.P. Roth, J.P. Klinman, Catalysis of electron transfer during activation of O2 by the flavoprotein glucose oxidase, Proc. Natl. Acad. Sci. USA 100 (2003) 62.
[18] Y.V. Geletii, C.L. Hill, R.H. Atalla, I.A. Weinstock, Reduction of O2 to superoxide anion (O2-)in water by heteropolytungstate cluster-anions, J. Am. Chem. Soc. 128 (2006) 17033.
[19] I.A. Weinstock, Outer-sphere oxidation of the superoxide radical anion, Inorg. Chem. 47 (2008) 404.
[20] W.A. Pryor, K.N. Houk, C.S. Foote, J.M. Fukuto, L.J. Ignarro, G.L. Squadrito, K.J. Davies, Free radical biology and medicine: it's a gas, man!, Am J. Physiol. Regul. Integr. Comp. Physiol. 291 (2006) R491.
[21] T. Nomura, Y. Matsuda, S. Takeyama, A. Matsuo, K. Kindo, J. Her, T. Kobayashi, Novel phase of solid oxygen induced by ultrahigh magnetic fields, Phys. Rev. Lett. 112 (2014) 247201.
[22] J.M. Alvarino, A. Chamorro, Continuous point groups: a simple derivation of the closed formula for the reduction of representations, J. Chem. Educ. 57 (1980) 785.
[23] J.D. Watts, R.J. Bartlett, A coupled-cluster study of inversion symmetry breaking in the F 2 molecular ion, J. Chem. Phys. 95 (1991) 6652.
[24] A.D. Becke, A new mixing of Hartree-Fock and local density-functional theories, J. Chem. Phys. 98 (1993) 1372.
[25] C. Lee, W. Yang, R.G. Parr, Development of the Colle-Salvetti correlation-energy formula into a functional of the electron density, Phys. Rev. B. 37 (1988) 785.
[26] T. Yanai, D.P. Tew, N.C. Handy, A new hybrid exchange–correlation functional using the Coulomb-attenuating method (CAM-B3LYP), Chem. Phys. Lett. 393 (2004) 51.
[27] M. Caricato, G.W. Trucks, M.J. Frisch, K.B. Wiberg, Oscillator strength: How does TDDFT compare to EOM-CCSD?, J Chem. Theory Comput. 7 (2010) 456.
[28] M.M. Francl, W.J. Pietro, W.J. Hehre, J.S. Binkley, M.S. Gordon, D.J. DeFrees, J.A. Pople, Self-consistent molecular orbital methods, XXIII: A polarization-type basis set for second-row elements, J. Chem. Phys. 77 (1982) 3654.
[29] A. McLean, G. Chandler, Contracted Gaussian basis sets for molecular calculations, I: Second row atoms, Z = 11–18, J. Chem. Phys. 72 (1980) 5639.
[30] K. Lopata, N. Govind, Modeling fast electron dynamics with real-time time-dependent density functional theory: application to small molecules and chromophores, J. Chem. Theory Comput. 7 (2011) 1344.
[31] S. Hirata, Tensor contraction engine: abstraction and automated parallel implementation of configuration-interaction, coupled-cluster, and many-body perturbation theories, J. Phys. Chem. A. 107 (2003) 9887.
[32] R.A. Kendall, E. Aprà, D.E. Bernholdt, E.J. Bylaska, M. Dupuis, G.I. Fann, R.J. Harrison, J. Ju, J.A. Nichols, J. Nieplocha, High performance computational chemistry: an overview of NWChem a distributed parallel application, Comput. Phys. Commun. 128 (2000) 260.
[33] H.D. Babcock, Internuclear distance in oxygen molecules, Proc. Natl. Acad. Sci. USA 23 (1937) 301.
[34] R.J. Celotta, R.A. Bennett, J.L. Hall, M.W. Siegel, J. Levine, Molecular photodetachment spectrometry, II: The electron affinity of O 2 and the structure of O 2, Phys. Rev. A: At. Mol. Opt. Phys. 6 (1972) 631.
[35] H. Nakatsuji, H. Nakai, Potential energy curves of dioxygen anion species, O- 2 and O 2–2, Chem. Phys. Lett. 197 (1992) 339.
[36] K.M. Ervin, I. Anusiewicz, P. Skurski, J. Simons, W.C. Lineberger, The only stable state of O2-is the X 2Πg ground state and it (still!) has an adiabatic electron detachment energy of 0.45 eV, J. Phys. Chem. A. 107 (2003) 8521.
[37] B.F. Minaev, Ab initio study of the ground state properties of molecular oxygen, Spectrochim. Acta Mol. Biomol. Spectrosc. 60 (2004) 1027.
[38] R. Celotta, R. Bennett, J. Hall, M. Siegel, J. Levine, Molecular photodetachment spectrometry, II: The electron affinity of O 2 and the structure of O 2−, Phys. Rev. A 6 (1972) 631.
[39] M. Musia, R.J. Bartlett, EOM-CCSDT study of the low-lying ionization potentials of ethylene, acetylene and formaldehyde, Chem. Phys. Lett. 384 (2004) 210.
[40] CRC Handbook of Chemistry and Physics, 85th ed., CRC Press, Boca Raton, Florida, 2005.
[41] R. Mulliken, Electronic population analysis on LCAO-MO molecular wave functions, IV: Bonding and antibonding in LCAO and valence-bond theories, J. Chem. Phys. 23 (1955) 2343.
[42] R.S. Mulliken, Electronic population analysis on LCAO–MO molecular wave functions I, J. Chem. Phys. 23 (1955) 1833.